





ORIGINAL ARTICLE

ATP6AP2-Related Disease Caused by Splicing Defects: Abnormal Glycosylation and the First Affected Female

¹AP-HP, Biochimie métabolique et Cellulaire, Hôpital Bichat, Paris, France | ²Paris Cité University, Xavier Bichat Medicine Department, Paris, France | ³Sorbonne Université, AP-HP, Department of Medical Genetics, Paris, France | ⁴Department of Neurology, Donders Institute for Brain, Cognition, and Behavior, Radboud University Medical Center, Nijmegen, the Netherlands | ⁵Department of Biochemistry and Genetics, Angers University Hospital, Angers, France | ⁶Translational Metabolic Laboratory, Department of Human Genetics, Radboud University Medical Center, Nijmegen, the Netherlands | ⁷Pedoneurology, Ampelokipoi, Athens, Greece | ⁸Paris-Saclay University, INSERM U1193, Orsay, France | ⁹Laboratory for Cytogenetics and Genome Research, Department of Human Genetics, KU Leuven, Belgium | ¹⁰Département Médicaments et Technologies Pour la Santé (DMTS), MetaboHUB, Université Paris-Saclay, CEA, INRAE, Gif sur Yvette, France | ¹¹INSERM U1231, Université Bourgogne Europe, Dijon, France | ¹²Laboratory for Molecular Diagnosis, Center for Human Genetics, KU Leuven, Leuven, Belgium | ¹³Center for Metabolic Diseases, University Hospital Gasthuisberg, KU Leuven, Leuven, Belgium | ¹⁴Pediatrics in Reference Center of Metabolic Diseases of ULSSA, Porto, Portugal | ¹⁵Unit for Multidisciplinary Research in Biomedicine, ICBAS, UP, Porto, Portugal

Correspondence: Arnaud Bruneel (arnaud.bruneel@aphp.fr) | Matthew P. Wilson (matthew.wilson@kuleuven.be)

Received: 8 April 2025 | Revised: 10 October 2025 | Accepted: 15 October 2025

Funding: This work was supported by FWO Senior Postdoctoral Fellowship, 1289023N; Jaeken-Theunissen CDG Fund; FWO-FNRS WEAVE program, G061524N; ERA-Net for Research on Rare Diseases, ERA-NET Cofund action; FWO GOI2918N; EUROGLYCAN-omics.

Keywords: ATP6AP2 | CDG | Golgi V-ATPase | MRXSH | XPDS

ABSTRACT

ATP6AP2 splicing variants cause syndromic X-linked intellectual disability Hedera type (XPDS; OMIM#300423) and X-linked parkinsonism with spasticity (MRXSH; OMIM#300911). Alternatively, ATP6AP2 missense variants lead to hepatopathy, immunological abnormalities, cutis laxa and only mild intellectual disability with N-/O-glycosylation defects (ATP6AP2-CDG; OMIM#301045). The disparity between neurological and hepatic ATP6AP2-related disease entities is an ongoing puzzle. We aimed to investigate whether patients with an isolated neurological presentation of ATP6AP2-related disease, consistent with XPDS/MRXSH, also have abnormal glycosylation biomarkers, potentially implicating this as part of the pathological mechanism. We identified three males and one female from three families with ATP6AP2 splicing variants and ID/DD, epilepsy, axial hypotonia, axonal neuropathy and microcephaly; the heterozygous female has a milder phenotype. RNA-Seq in patient-derived fibroblasts validated defective splicing, correlated with lowered ATP6AP2 protein levels in fibroblasts alongside glycosylation abnormalities. We describe defective glycosylation alongside ATP6AP2 splicing variants in four patients, including the first female with ATP6AP2-related disease. This connects more closely the phenotypes of XPDS/MRXSH and ATP6AP2-CDG and indicates that abnormal glycosylation markers may be a consistent feature of splicing variants, and potentially part of the pathological mechanism underlying ATP6AP2-related disease caused by abnormal splicing. We also provide additional evidence that neurodevelopment is uniquely sensitive to the gene dosage of ATP6AP2, linked to the isolated neurological phenotype found in patients with splice variants and the attenuated, but still severe, phenotype of the female in our study. Glycosylation defects can be found in "splicing" forms of ATP6AP2-related diseases, bridging the gap between XPDS, MRXSH and ATP6AP2-CDG.

© 2025 SSIEM.

1 | Introduction

Congenital disorders of glycosylation (CDG) are a group of inherited metabolic diseases characterized by faulty protein or lipid glycosylation. To date, over 180 causative genes have been identified [1]. A subgroup of CDG is characterized by defects of V-ATPase, a proton pump which mediates the acidification of diverse intracellular compartments [2]. Recessive or X-linked pathogenic variants in genes encoding V-ATPase subunits cause variable phenotypes including immunodeficiency, epilepsy, developmental delay (DD)/intellectual disability (ID), renal disease, deafness, hepatopathy and/or cutis laxa [3–12]. In several of these disorders, impaired Golgi trafficking has been identified, in combination with disrupted processing of N- and O-glycans [13].

ATP6AP2 was previously a protein of controversial function. Long thought to act as a prorenin receptor at the cell surface, this assumption remains doubtful after two decades of research [14]. Nowadays, overwhelming evidence points toward the main role of ATP6AP2 being a chaperone protein, alongside ATP6AP1, involved in the assembly of the V-ATPase protein pore (V0) domain [14, 15]. However, only the C-terminal fragment of ATP6AP2, after cleavage by furin in the Golgi apparatus, is found embedded in the functional V-ATPase. The possibility remains that the N-terminal fragment of ATP6AP2 has another molecular role [15, 16].

Pathogenic *ATP6AP2* variants were first described by Hedera et al. in 2002 and in the termed Syndromic X-linked intellectual disability Hedera type (MRXSH, OMIM #300423) [8]. In 2013, Korvatska et al. expanded the group of ATP6AP2-related diseases to include X-linked parkinsonism with spasticity (XPDS, OMIM #300911), characterized by variable-onset neurodegeneration [4]. In both MRXSH and XPDS, only hypomorphic splice variants with partial exon-skipping have been identified. Subsequently, in 2017, Rujano et al. described three individuals with hemizygous missense variants in *ATP6AP2*, associated with defective glycosylation, hepatopathy, recurrent infections, cutis laxa, and milder/absent neurological symptoms [7]. This disease was named ATP6AP2-CDG (OMIM #301045).

Here, we report on four affected individuals, including the first described female, with *ATP6AP2* hypomorphic splice variants, reduced ATP6AP2 protein levels in fibroblasts, severe neurological phenotypes and, interestingly, glycosylation defects in serum. This offers new insight into phenotype–genotype correlation in ATP6AP2-related disorders, and bridges the gaps between XPDS, MRXSH and ATP6AP2-CDG.

2 | Materials and Methods

2.1 | Genetic Studies

2.1.1 | Genome Sequencing

Patients 1 and 2 (P1 and P2) were investigated via exome and/or genome sequencing as part of a cohort of individuals with biomarkers indicative of CDG [17]. Filtering and variant curation were prioritized based on the analysis of known or predicted CDG-associated genes.

For patients 3 and 4 (P3 and P4), quatuor-based genome sequencing was performed at the SeqOIA laboratory (Paris, France). DNA was extracted from blood cells, and fragmented using sonication (LE220plus, Covaris). Libraries were prepared using the PCR-free protocol NEBNext Ultra II End repair/A-tailing module & Ligation module, New England Biolabs. Paired-end (2x150) sequencing was performed on Flow Cell S4, NovaSeq 6000, Illumina. Raw output was demultiplexed (bcl2fastq, v2.20.0.422, Illumina) and aligned on the GRCh38 reference genome using BWA-MEM, 0.7.15. Duplicates were marked using Picard Mark Duplicates (2.8.1), base quality was recalibrated with GATK4 (v4.1.6.0, Broad Institute). Small variants were called using GATK4 (v4.1.7.0, Broad Institute) and annotated by SNPeff (4.3t), SnpSift (4.3t). Structural variants were called with ClinSV (1.0) and annotated by AnnotSV (v3.0.7). An average depth-of-coverage of 37x and 42x was obtained for the two probands, and variants were prioritized according to impact, frequency, and segregation.

2.1.2 | RNA Sequencing

For P1 and P2, RNA-seq was performed using total RNA extracted from fibroblasts. Quality control was carried out using the RNA 6000 Nano Assay on a Bioanalyzer 2100 (Agilent). Libraries were prepared using the TruSeq stranded mRNA Sample Prep Kit (Illumina) and sequenced on a NovaSeq 6000 (Illumina). After demultiplexing and mapping with STAR 2.6.1 to the hg38 genome assembly, samples (a total of 27 including P1 and P2) were processed using DROP 1.2.4 to detect aberrant splicing or gene expression, as well as monoallelic expression of rare variants [18, 19]. Reads were mapped to hg38 and visualized using Integrative Genomics Viewer [20]. Normalized read counts across the *ATP6AP2* gene were calculated using featureCounts v2.1.1 to compute total reads at the ENSG00000182220.15 (AT6AP2) locus, followed by normalization with DESeq2 in Bioconductor version 3.21 (BiocManager 1.30.26), inside Rstudio v4.5.1.

For P3 and P4, RNA was extracted from fibroblasts, using the RNeasy plus mini kit (Qiagen). Cells were treated or not with a nonsense-mediated decay (NMD) inhibitor (either cycloheximide or emetine). Reverse transcription was performed using the SuperScript III first strand kit (Life Technologies). RNA sequencing was performed using the mRNA stranded kit (Illumina). Strand-specific sequencing libraries were prepared using Illumina Stranded mRNA Prep. Paired-end 75-bp sequencing was performed on NextSeq 500 Illumina platform, demultiplexing and raw sequences were obtained using Illumina's bcl2fastq. Reads were mapped and visualized as described for P1 and P2. Global quality was assessed using FastQC, RNA-SeQC, Picard Tools and MultiQC. Splicing alterations were detected using Fraser [21].

RT-qPCR analysis was performed as previously [22]. Briefly, transcribed DNA corresponding to *ATP6AP2* (NM_005765.3) was compared to *HPRT* (NM_000194) after extraction using a Qiagen RNAeasy kit (74104) transcription using a First Strand cDNA Synthesis Kit (Life Technologies, K1612) and analysis using the 2× LightCycler 480 SYBR Green I Master kit. Data were analyzed using the LightCycler 480 Software (Roche Applied Science). Primers used can be found in Table S2.

2.1.3 | Chromosome X Inactivation Skewedness

In P4, chromosome X inactivation skewedness was evaluated by analysis of methylation status in loci of PCSK1N (Xp11.23), HUMARA (Xq11.2-2q12), ZDHHC15 (Xq13.3) and SLITRK4 (Xq27.3) in peripheral blood mononuclear cells (PBMC). The inactivation ratio at the HUMARA locus serves as the reference. A ratio <80/20% corresponds to random chromosome X inactivation ($\sim90\%-95\%$ of females in general population); between 80/20% and 90/10% corresponds to a bias ($\sim5\%-10\%$ of females); >90/10% corresponds to a strong bias (1%-5% of females). Of note, this method cannot distinguish which chromosome X is preferentially (in)activated.

2.2 | Cellular Studies

2.2.1 | Cell Culture

Primary fibroblasts from affected individuals and controls were grown from skin biopsies. Fibroblasts were cultured in DMEM/F12 (Life Technologies) supplemented with 10% FBS (Clone III, HyClones). HEK293 cells were cultured in the same conditions but using DMEM as the culture medium.

2.2.2 | Immunoblotting

Immunoblotting was performed as previously described [23]. Signal detection was performed by autoradiography with an Amersham ImageQuant 800 (Cytiva). Quantification was performed with the ImageJ software package. All antibodies used for immunoblotting, as well as the immunogenic peptides used to raise them, can be found in Table S1.

2.2.3 | siRNA Knockdown of ATP6AP2

HEK293 cells were seeded in six-well plates in DMEM (Gibson)+10% FBS and were immediately retrotransfected with siRNA complementary to ATP6AP2 mRNA (Sigma EHU106681) alongside the RNAiMAX reagent (Invitrogen). For each well, 150 μ L of DMEM without serum and 9 μ L of RNAiMAX were mixed with 150 μ L of DMEM and 40 pmol of siRNA. After 5 min, 300 μ L of the final mix was added, dropwise, to each well. The cells were then incubated for 24 h before the collection of protein lysates as described above.

2.2.4 | Autophagic Flux Assay in Cultured Skin Fibroblasts From P3

Skin fibroblasts from P3 and from two healthy controls were cultured in DMEM supplemented with 10% FBS, and penicil-lin/streptomycin (100 U/mL); 200,000 cells were seeded per well of a six-well plate. Two days later, the culture medium was refreshed, and the cells were treated with 1 μ M of the mTOR inhibitor PP242 (Tocris, 4257) for 3 h and 100 nM of the V-ATPase inhibitor Bafilomycin A1 (BafA1, Tocris, 1334) for 1 h alone or combined (BafA1 was added during the last hour of PP242 treatment). The cells were then lysed in RIPA buffer containing

protease inhibitors (Sigma-Aldrich, P8340) and phosphatase inhibitors (Sigma-Aldrich, P0044), and 15 µg of total proteins were analyzed by western blot. Briefly, proteins were separated by SDS-PAGE on 15% acrylamide gels before transfer onto PVDF membranes. Membranes were blocked in 5% bovine serum albumin in TBS (20 mM Tris, 137 mM NaCl, pH 7.6) containing 0.1% Tween 20. Antibodies against LC3 (Cell Signaling Technology, 4108, 1:1000 dilution) and HSC70 (Santa Cruz Biotechnology, sc-7298, 1:1000) were added to the blocking buffer overnight at 4°C. Secondary antibodies were diluted in blocking buffer and added for 1h at room temperature before chemiluminescence detection (Pierce ECL Western Blotting Substrate, Thermo Scientific, 33,209) and imaging using the Invitrogen iBright CL1500 Imager. Densitometry analysis was performed using ImageJ software to determine LC3-II:LC3-I ratios. Statistical analysis was performed using Prism software.

2.3 | Glycosylation Studies

2.3.1 | N-Glycosylation

In P1 and P2 high-resolution mass spectrometry of the intact transferrin was performed as described previously [24]. $5\,\mu L$ of serum sample was incubated with anti-transferrin beads before injection for immunoprecipitation. The eluate was analyzed on an Agilent 1260 nano LC-HPLC-chip system using a C8 protein chip coupled to an Agilent 6540 QTOF LC/MS system (Agilent Technologies). Data analysis was performed using Agilent Mass Hunter Qualitative Analysis Software B.05 and an in-house developed reporting workflow was used for data analysis. Data are represented as percentages compared to the transferrin protein with two intact biantennary N-glycans.

In P3 and P4, N-glycosylation was studied by capillary electrophoresis of serum transferrin using a Sebia kit and by two-dimensional electrophoresis (2-DE) of serum haptoglobin, as previously described [25]. Isoelectric focusing (IEF; first dimension) was performed on a ZOOM strip (pH4-7; Thermo Fisher Scientific) followed by SDS-PAGE (second dimension) on a NuPAGE Bis-Tris gel (4%–12%; Thermo Fisher Scientific), transfer onto a nitrocellulose membrane, and incubation with an anti-haptoglobin antibody (1/3000 v/v; Siemens Healthineers). Detection was performed using the Clarity ECL reagent (Bio-Rad) and images were acquired on a XRS Chemidoc camera (Bio-Rad).

2.3.2 | Core 1 Mucin-Type O-Glycosylation

In P1 and P2 apoC-III IEF was performed as described previously with small modifications to assess core 1 mucin-type O-glycosylation [26]. $2\mu L$ of serum/plasma were diluted 15-fold with saline solution. The gel was rehydrated in a solution containing 8M urea before electrophoresis and blotting on nitrocellulose membrane filter. The blot was washed and blocked before incubation with anti-apoC-III (1/2000, Rockland). After incubation with the secondary anti-goat-HRP antibody (1/5000, Thermo Scientific) and ECL reagent (Pierce), the blot was visualized on a LAS3000 imaging system (Fujifilm) and quantified with ImageQuant software.

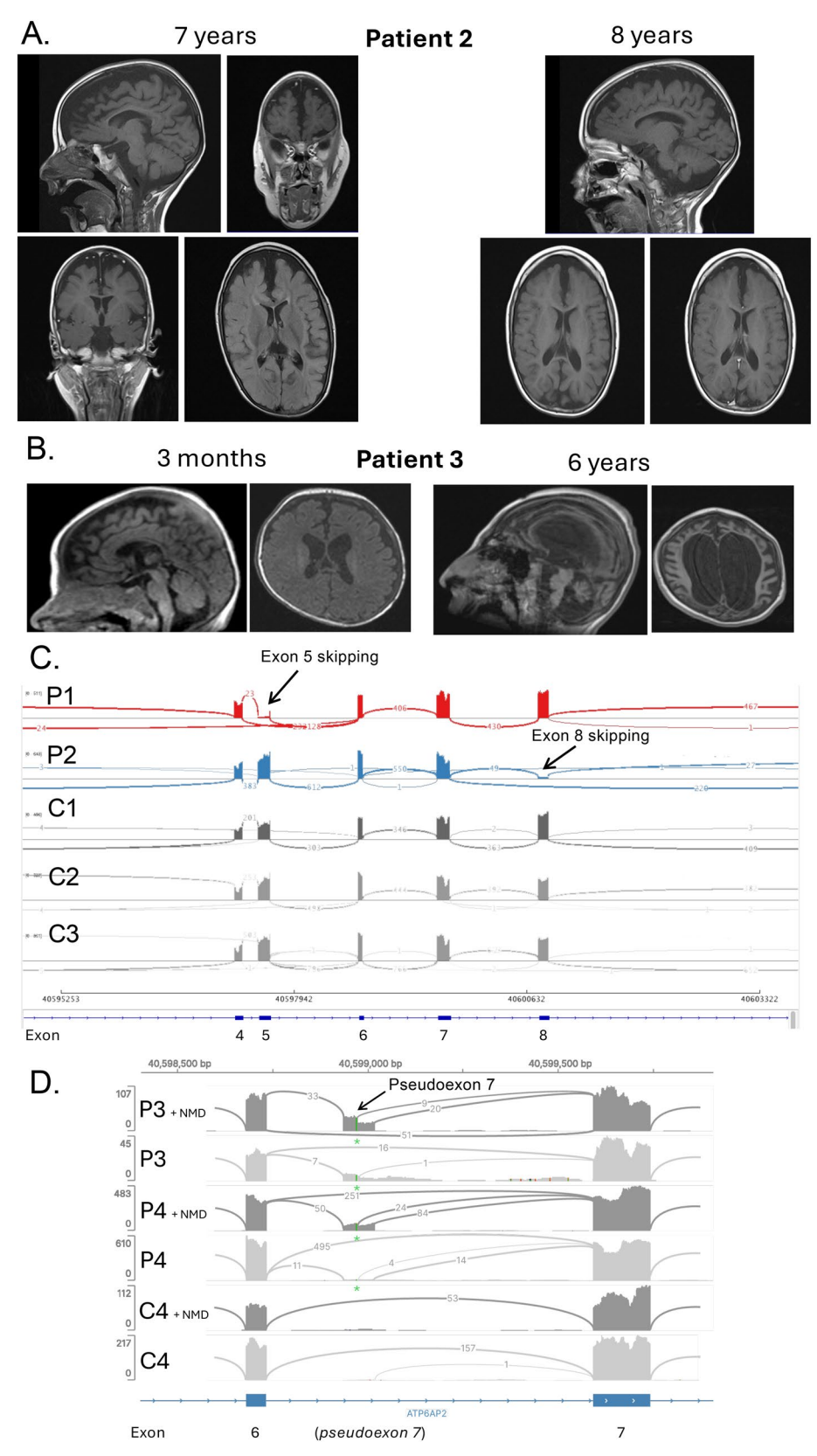


FIGURE 1 | Legend on next page.

In P3 and P4, core 1 mucin-type O-glycosylation was studied by 2-DE of apoC-III, as previously described [27]. The same 2-DE protocol as that of haptoglobin was performed (see above), except

for the primary antibody (anti-apoC-III antibody, 1/5000 v/v; Meridian Bioscience). Control ranges (Table 3) were established during clinical diagnostic use, as described previously [28, 29].

FIGURE 1 | Clinical and *ATP6AP2* RNA-Seq data from P1-4. (A) MRI images of P2, initially performed at age 4, with follow-up images at ages 7 and 8 (shown here), reveal enlarged subarachnoid spaces symmetrically affecting both hemispheres, most prominently in the frontal, parietal, and temporal lobes. The scans also showed reduced white matter volume, increased dimensions of the lateral and third ventricles without expansion of the fourth ventricle, and a thin corpus callosum, brainstem, and cerebellum. (B) Brain MRI in P3 showed progressive cortico-subcortical and cerebellum atrophy between the ages 3 months and 6 years. (C) Sashimi plot of ATP6AP2 mRNA obtained from RNA-Seq data from fibroblasts of patients 1 and 2 (P1 and P2) and three controls (C1-3). Strong skipping of exon 5 (> 90%; P1) and exon 8 (> 75%; P2) compared to controls can be observed in the affected individuals (arrows). (D) Sashimi plot of ATP6AP2 mRNA obtained from RNA-Seq data from fibroblasts of Individuals 3 and 4 (P3 and P4) and a male control (C4), with or without the use of a nonsense-mediated decay (NMD) inhibitor. Partial retention of pseudoexon 7 can be observed in P3 and P4 (arrows). This partial retention is increased upon inhibition of NMD. The premature stop codon found in pseudoexon 7 is marked with a green asterisk. For details of altered splicing junctions see supplementary information.

3 | Results

3.1 | Clinical Features

P1 is a 15-year-old male, born from unrelated Portuguese parents after a 36-week pregnancy. He experienced significant growth delay, microcephaly, facial dysmorphism, absent language and non-independent walking. He experienced hypertonia and epileptic episodes, now under control receiving four antiepileptic drugs. Brain magnetic resonance imaging (MRI) was normal at 4 and 11 months. Routine laboratory testing revealed an increased blood aspartate aminotransferase activity (72 UI/l; reference < 40) and mild hyperlactatemia (5.3 mmol/L; reference: 0.6–2.4). Genetic testing uncovered a previously unreported hemizygous c.397-3_397-2del variant in *ATP6AP2*, inherited from his heterozygous mother.

P2 is a 14-year-old male, conceived via IVF and born prematurely after 31 weeks of pregnancy. He has a history of severe growth delay, DD and ID, axial hypotonia with an inability to sit independently, scoliosis, and severe epilepsy poorly controlled with valproic acid and levetiracetam, dysmorphic facial features and microcephaly. Brain MRI performed at four years revealed leukomalacia, with follow-up at 7 and 8 years (Figure 1A). Genetic testing uncovered a hemizygous c.858G>A (p.Ala286=) in ATP6AP2. Genetic material from the father and anonymous oocyte donor were unavailable. The variant had previously been reported by Liang et al. in another individual with a similar clinical picture [30]. The effect of this variant on ATP6AP2 splicing had been assessed by Liang et al. using a minigene assay and was found to lead to skipping of exon 8.

P3 and P4 are siblings of Caucasian origin, whose parents are unrelated. P3, a 10-year-old male, has a history of major ID with an absence of psychomotor development, severe neonatal epileptic encephalopathy, axial hypotonia, diaphragmatic paralysis, axonal neuropathy and progressive microcephaly. Brain MRI (Figure 1B) showed progressive cortico-subcortical and cerebellum atrophy between the ages of 3 months and 6 years. P4, a 14-year-old female, has a history of mild ID, autism and progressive microcephaly. Her brain MRI was normal at 10 months. Neither P3 nor P4 had any evidence of liver involvement. Biochemically, they had normal coagulation factors concentrations, copper, ceruloplasmin and cholesterol. Genetic testing uncovered a previously unreported *de novo* c.588+237G>A variant in *ATP6AP2* (hemizygous in P3; heterozygous in P4). The recurrence of this *de novo* variant in two siblings is thought to result from germinal mosaicism in the mother.

For all patients, clinical information and comparison to previously reported ATP6AP2-CDG patients is presented in Table 1. Images of P2, P3 and P4 (Figure S1) and full clinical histories of all individuals are available in the Supporting Information.

3.2 | Splicing Variants in *ATP6AP2* Lead to Decreased RNA and Protein Expression

3.2.1 | RNA-Seq Analysis in Fibroblasts From P1-P4 Shows Altered Splicing of *ATP6AP2*

Fibroblasts derived from P1-4 and four controls (C1-4) were analyzed by RNA-Seq. In P1 harboring the c.397-3_397-2del variant, close to the canonical splice acceptor site of exon 5, > 90% of reads were found to skip exon 5 (Figure 1C). This is predicted to lead to an in-frame deletion of 138 nucleotides in the corresponding mature mRNA, and presumably a truncated protein product, missing 46 amino acids (Arg133 to Glu178) (Figure 2). In P2, hemizygous for c.858G>A (p.Ala286=), a similar in-frame skipping of 120 nucleotides corresponding to exon 8 was identified in >75% of transcripts, removing 40 amino acids (Phe247 to Ala286) (Figures 1C and 2). Additionally, RT-qPCR analysis from RNA extracted from fibroblasts of P2 showed a 38% reduction in transcript levels compared to three controls, assessed using primers spanning exons 1 and 2 of the canonical full-length (NM_005765.3) ATP6AP2 transcript (Figure S2A). RT-qPCR using primers spanning the exon 7-8 boundary showed a dramatic reduction to 4% of the expression in the same three controls (Figure S2B).

P3, hemizygous for the c.588+237G>A variant in the intronic region between exons 6 and 7, showed partial inclusion of a pseudoexon encoding 10 amino acids before ending in a stop codon introduced by the c.588+237G>A substitution itself (~30% of reads). This also presumably resulted in a truncated protein product consisting of only the first 206 amino acids (Figures 1D and 2). The inhibition of nonsense-mediated decay (NMD) resulted in increased retention of this pseudoexon, which was included in ~30%-40% of reads spanning the exon 6/pseudoexon 7 junction. In P4, the c.588+237G>A heterozygous sister of P3, a weak inclusion of the pseudoexon (~2%-4% of reads) was identified in untreated fibroblasts. The inhibition of NMD resulted in stronger inclusion, to ~16%-30% reads (Figure 1D). These results confirmed that, in all individuals, the variants identified resulted in aberrant splicing of *ATP6AP2*. Of note,

15732665, 2025. 6, Downloaded from https://onlinelibrary.vikey.com/obi710.1002 jimd.70109 by Assistance Publique Hopitaux De Paris Ap-Hp, Wiley Online Library on [23/10/2025]. See the Terms and Conditions (https://onlinelibrary.vikey.com/ebi710.1002 jimd.70109 by Assistance Publique Hopitaux De Paris Ap-Hp, Wiley Online Library on [23/10/2025]. See the Terms and Conditions (https://onlinelibrary.vikey.com/ebi710.1002 jimd.70109 by Assistance Publique Hopitaux De Paris Ap-Hp, Wiley Online Library on [23/10/2025]. See the Terms and Conditions (https://onlinelibrary.vikey.com/ebi710.1002 jimd.70109 by Assistance Publique Hopitaux De Paris Ap-Hp, Wiley Online Library on [23/10/2025]. See the Terms and Conditions (https://onlinelibrary.vikey.com/ebi710.1002 jimd.70109 by Assistance Publique Hopitaux De Paris Ap-Hp, Wiley Online Library on [23/10/2025]. See the Terms and Conditions (https://onlinelibrary.vikey.com/ebi710.1002 jimd.70109 by Assistance Publique Hopitaux De Paris Ap-Hp, Wiley Online Library on [23/10/2025]. See the Terms and Conditions (https://onlinelibrary.vikey.com/ebi710.1002 jimd.70109 by Assistance Publique Hopitaux De Paris Ap-Hp, Wiley Online Library on [23/10/2025]. See the Terms and Conditions (https://onlinelibrary.vikey.com/ebi710.1002 jimd.70109 by Assistance Publique Hopitaux De Paris Ap-Hp, Wiley Online Library on [23/10/2025]. See the Terms and Conditions (https://onlinelibrary.vikey.com/ebi710.1002 jimd.70109 by Assistance Publique Hopitaux De Paris Ap-Hp, Wiley Online Library on [23/10/2025]. See the Terms and Conditions (https://onlinelibrary.vikey.com/ebi710.1002 jimd.70109 by Assistance Publique Hopitaux De Paris Ap-Hp, Wiley Online Library on [23/10/2025]. See the Terms and Conditions (https://onlinelibrary.vikey.com/ebi710.1002 jimd.7010.1002 ji

 TABLE 1
 Clinical information from previously reported ATP6AP2-CDG patients and the cases from this report.

This study patient 4		12 years	Female	c.588+237G>A			+	Mild	I	Normal			ı		ı	I	I	
This study patient 3		8 years		c.588+237G>A	Splice		+	Severe	+ (50dB)	Cortico-subcortical and cerebellum atrophy			I		ı	I	I	Transient during ketogenic diet
This study patient 2		14 years		c.858G>A; p.Ala286=	3 1		+	Severe	I	Leukomalacia, decreased white matter	+		I	ı	ı	ı		
This study patient 1		15 years		c.397-3_397-2. del			+	Severe	I	Normal	+		Mildly increased AST			I		
Fang et al. patient 1		21 months	Male	c.185G>A; p.Gly62Glu			I	+	I				+ (cirrhosis)		+	ı	+	Hypercholesterolemia with increased LDL-cholesterol
Rujano et al. patient 3		17 years		c.293C>T; p.Leu98Ser	Missense		I	I	I	N/A	N/A		+ (cirrhosis)	+	+	+	+	Hypercholestero- lemia
Rujano et al. patient 2		10 months		c.212G>A; p.Arg71His		St	I	Mild	I		+		+	+	+	+	+	Mildly increased LDL- cholesterol
Rujano et al. patient 1	data	21 years		c.212G>A; p.Arg71His		nental sympton	I	Mild	ı		Mild		+ (cirrhosis)	+	+	+	+	1
	Demographic and genetic data	Age	Sex	ATP6AP2 variant (NM_005765.3/ ENST00000636580.2)	Variant type	Neurological and developmental symptoms	Epilepsy	Intellectual disability/ developmental delay	Hearing loss	Brain MRI	Facial dysmorphism	Other symptoms	Hepatopathy	Splenomegaly	Cutis laxa	Recurring infections	Abnormal coagulation testing	Dyslipidemia

TABLE 1 | (Continued)

	Rujano et al. patient 1	Rujano et al. patient 2	Rujano et al. patient 3	Fang et al. patient 1	This study patient 1	This study patient 2	This study patient 3	This study patient 4
Copper/ ceruloplasmin	N/A	Decreased serum copper; normalized	Normal serum copper	Decreased ceruloplasmin			Normal	Normal
Glycosylation studies								
Serum transferrin		Type II profile		N/A (a)		Type II pr	Type II profile (mild)	
Serum apoC-III		N/A		N/A		apoC-II	$apoC-III_1$ profile	
Serum N-glycome/ glycoproteomics	Hypo- sialylation		N/A		N/A	N/A	Discrete hyposialylation	ialylation

Abbreviations: ApoC-III: apolipoprotein C-III; AST: aspartate aminotransferase; m.o.: months old; MRI: magnetic resonance imaging; N/A: not available; y.o.: years old The authors stated that the serum transferrin glycosylation study was not performed because the patient underwent liver transplantation. RNA-Seq performed on whole blood in P4 only showed a very weak splicing alteration. In concordance with this result, the X-chromosome inactivation study in PBMC revealed a skewed X-inactivation (82%–18%).

3.3 | ATP6AP2 Protein Levels Are Reduced in P1-4

To assess if the abnormal splicing identified in P1-4 had an impact on ATP6AP2 protein levels, immunoblotting was performed from patient-derived dermal fibroblasts. The 39.0 kDa ATP6AP2 protein is processed in two ways: firstly, 16 amino acids (1.6 kDa) at the N-terminus are removed, constituting the signal peptide, leaving a protein of 37.4 kDa, the most abundant ATP6AP2 polypeptide in the cell. This form can also be subsequently cleaved by furin at Arg278, part of a KTR*TI motif, leaving N-terminal and C-terminal fragments of 29.0 and 8.4 kDa, respectively [7, 31]. To confirm that we could detect reduced levels of ATP6AP2 protein, siRNA was used to knock down ATP6AP2 in HEK293T cells. Indeed, the major (37.4 kDa; without signal peptide) and N-terminal fragments were reduced to 16.1% and 24.9% of control levels, respectively, upon siRNA transfection (Figure 3A).

In control fibroblasts (C5-7), we were able to detect full-length ATP6AP2 protein (39.0 kDa), ATP6AP2 with the signal peptide cleaved (37.4kDa), and the N-terminal fragment after furin cleavage (29.0 kDa) (Figure 3B). In fibroblasts from affected individuals (P1-4) compared to three control fibroblasts (C5-7), levels of the major (37.4 kDa) ATP6AP2 protein product, where the signal peptide has been cleaved, were reduced to 15.4%, 25.2%, 34.7%, and 30.1% of control levels in P1-4, respectively. Intriguingly, in P1 and P2, additional band(s) could be visualized above the molecular weight of the 29.0 kDa N-terminal fragment band identified in control cells. These likely represent truncated forms of ATP6AP2 produced by the in-frame deletions of exons 5 and 8, respectively. In P3 and P4, no bands at molecular weights differing from those in control fibroblasts could be identified. This indicates both that the truncated mRNA undergoes NMD, as shown in RNA-Seq results, and that the protein product is degraded post-translationally. The uncropped Western blot images are available in Figure S3.

In P1 and P2, >90% and >75% of reads were found to skip exons 5 and 8, respectively. The fact that the full-length form of ATP6AP2 was still the predominant protein isoform in these patients suggested that, perhaps, the overall transcript output may be elevated in these patients as part of a compensatory mechanism. This was however, refuted by RT-qPCR results from fibroblasts of P2, where a reduction of 38% compared to controls was identified when using primers between exons 1 and 2, distal to the skipped exon 8 in aberrant transcripts (Figure S2). In addition, DESeq2-normalized transcripts showed total reads across ATP6AP2 to be similar, or lower, than the mean of all 27 samples analyzed in the same RNA-Seq experiment (P1: 3837; P2: 4970; mean of all samples: 4885). Together with the lower total protein levels of fulllength ATP6AP2 in fibroblasts in P1 and P2, this indicated that the truncated forms of protein lacking exons 5 and 8, respectively, are probably largely degraded after protein translation,

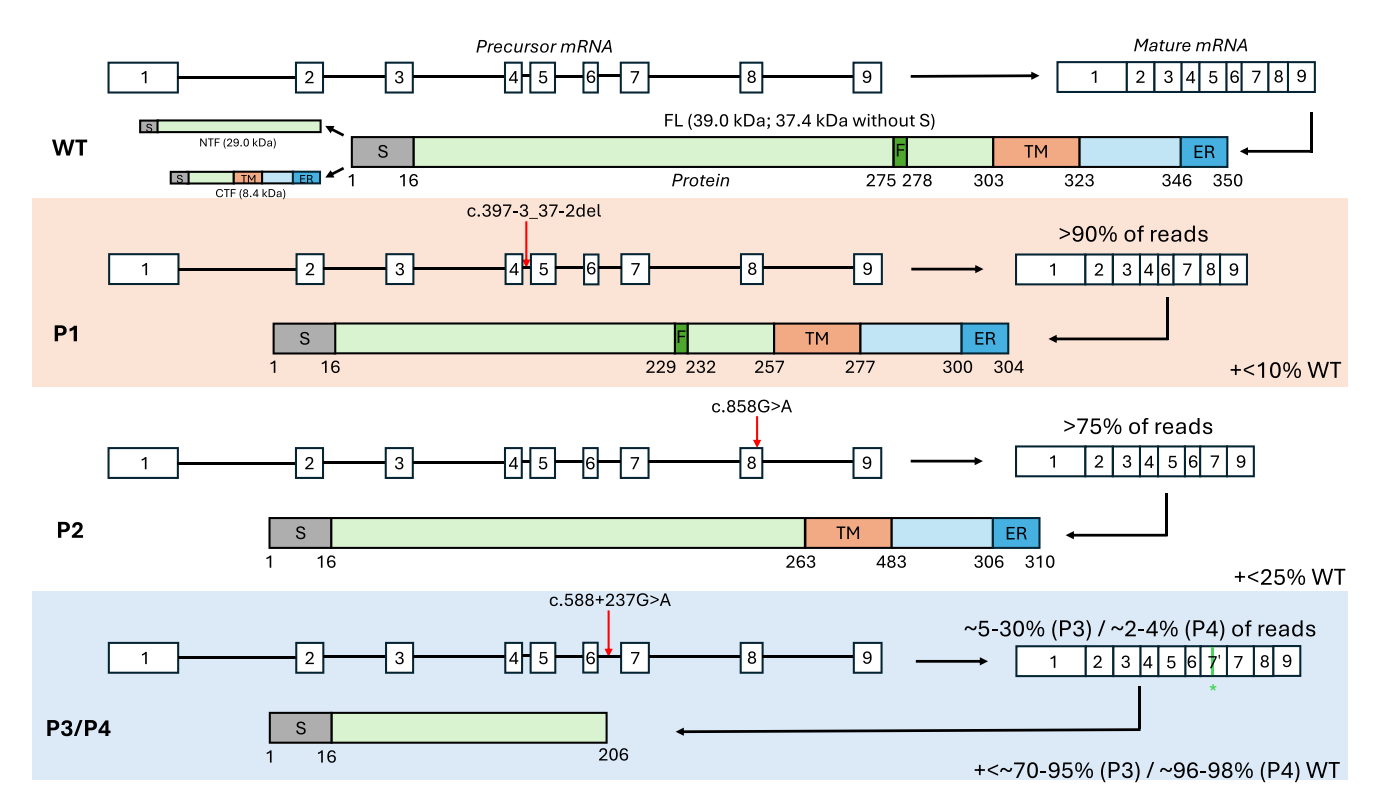


FIGURE 2 | Expected protein products resulting from the *ATP6AP2* splicing variants in P1-4. Top of figure: Wild-type (WT) pre-mRNA, mature mRNA and protein product of the reference *ATP6AP2* transcript (reference sequence: NM_005765.3/ENST00000636580.2). In P1, the c.397-3_397-2del variant is predicted to lead to an in-frame deletion of 138 nucleotides in the mature mRNA, and presumably in a truncated protein product missing 46 amino acids (Arg133 to Glu178). In P2, the c.858G>A (p.Ala286=) variant is predicted to lead to a similar in-frame skipping of 120 nucleotides corresponding to exon 8, expected to remove 40 amino acids (Phe247 to Ala286). In patients 3 and 4 (P3 and P4), the c.588+237G>A variant resulted in partial inclusion of the out-of-frame pseudoexon 7 (7' in the figure) including a stop codon after 11 amino acids are encoded (shown as a green bar and asterisk), expected to result in a truncated protein product consisting of only the first 206 amino acids. Note that this alternative mRNA is probably the target of NMD, as suggested by RNA-Seq results presented in Figure 1D. CTF: C-terminal fragment; ER: endoplasmic reticulum retention motif; F: furin cleavage site; FL: full-length protein; NTF: N-terminal fragment; S: signal peptide; TM: transmembrane domain.

and that *ATP6AP2* transcription is not significantly altered. Alternatively, it is possible that the antibody used for western-blotting binds more poorly to the truncated proteins than to the full-length protein, since the immunogenic peptide includes 8 amino acids from exon 5 and 40 amino acids from exon 8 (see Table S1).

In summary, these results showed that the splice site variants in P1 and P2, and the induction of a cryptic splice site by the deep intronic variant in P3 and P4, reduce ATP6AP2 protein levels in fibroblasts, likely leading to insufficient protein levels to sustain efficient V-ATPase complex assembly and function.

Previous studies have shown an increased sensitivity to the V-ATPase complex inhibitor Bafilomycin $\rm A_1$ in ATP6AP2-depleted cell lines, indicated by a relatively high ratio of LC3-II/LC3-I upon treatment [32, 33]. This was not the case in fibroblasts from P3 (Figure S4). However, there was evidence of reduced autophagic flux, indicated by a reduced LC3-II/LC3-I ratio after induction of autophagy using the mTOR kinase inhibitor PP242 and subsequent treatment with the V-ATPase complex inhibitor Bafilomycin $\rm A_1$.

3.4 | Glycosylation Studies Reveal Abnormal Protein N- and O-Glycosylation

In P1-4, the study of transferrin glycoforms displayed Nglycosylation defects with profiles evocative of V-ATPase defects (Table 2). A noticeable reduction of the disialylated glycan chain, the predominant form in healthy individuals, was observed. Additionally, all patients showed an increase in glycan chains with one or no sialic acids. In three out of four patients (P1-3), glycan chains lacking one galactose, and thus also one sialic acid, were also evident. For P1, P2, and P4, a combined loss of two sialic acids and one galactose was apparent. Moreover, in P1, low percentages of transferrin glycoforms with a loss of two or three galactoses, and thus also two or three sialic acids, were detected. To illustrate these glycosylation data, the mass spectrum of transferrin from P1, who exhibits the most severe biochemical phenotype, showed notable differences compared to the control spectrum characteristic for all patients (Figure 4A); additional peaks were observed corresponding to the loss of terminal sialic acid and galactose residues from the glycan structures. These structural changes were compatible with Golgi homeostasis defects, including V-ATPase defects [7, 34, 35].

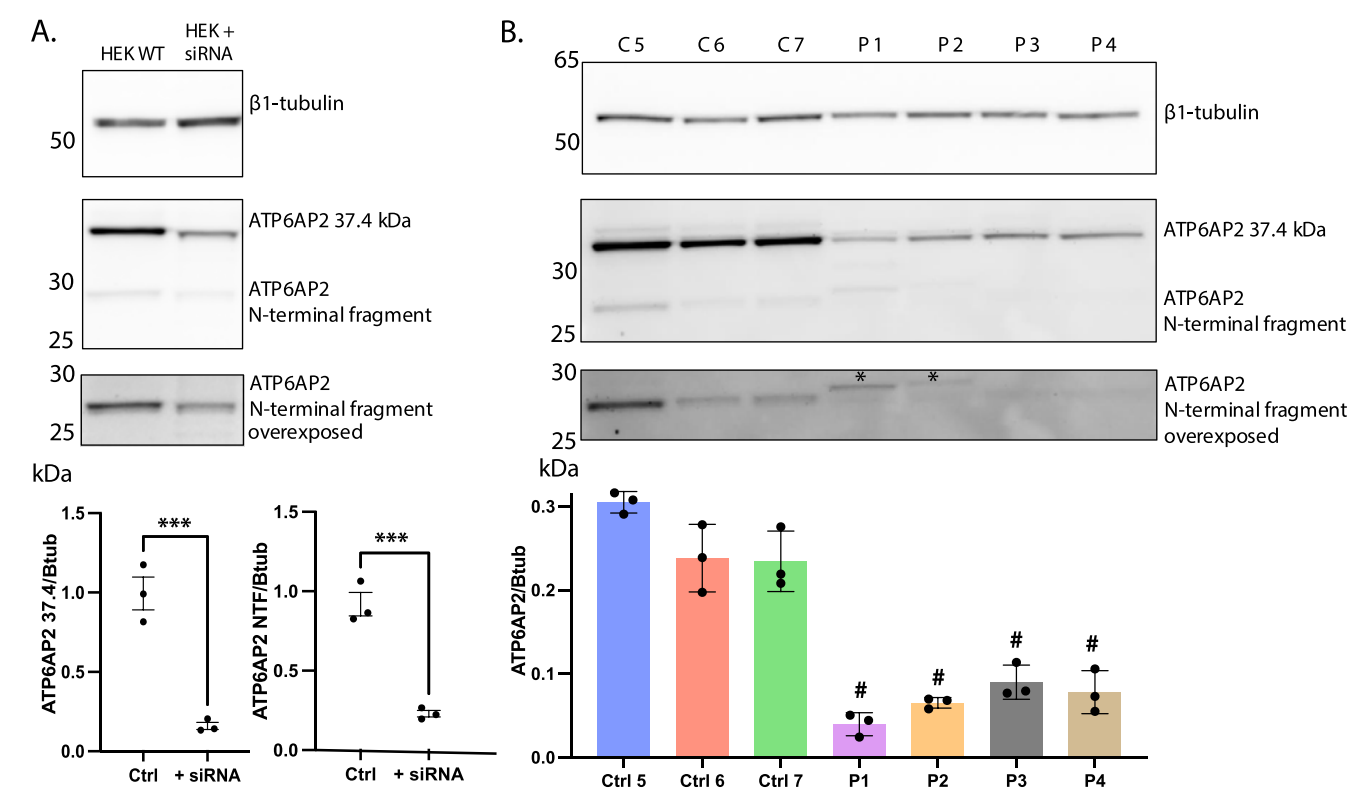


FIGURE 3 | ATP6AP2 protein levels are reduced in the fibroblasts of P1-4. (A) Inhibition of ATP6AP2 mRNA by siRNA in HEK293 cells confirms siRNA-mediated knockdown of ATP6AP2 levels. ***=p < 0.001 by one-way ANOVA. (B) In fibroblasts from P1-4 compared to three control fibroblasts (C5-7), levels of the full-length (without signal peptide) ATP6AP2 protein product were reduced to 15.4%, 25.2%, 34.7% and 30.1% in P1, P2, P3 and P4, respectively. In P1 and P2, additional band(s) could be visualized above the molecular weight of the N-terminal fragment band found in control cells (marked with *), possibly representing truncated forms of ATP6AP2 produced by the in-frame deletions of exons 5 and 8, respectively. In P3 and P4, no bands at molecular weights differing from those in control fibroblasts could be identified, indicating that both that the truncated mRNA undergoes NMD, as shown in RNA-Seq results (Figure 1), and that the protein product is degraded post-translationally. #=p < 0.0001 compared to one-way ANOVA analysis with each individual control.

In contrast, the control exhibits a more uniform glycan profile, with minimal sialic acid loss, remaining within the control range of less than 8%. The additional peaks in the patient spectrum likely reflect incomplete glycosylation processing or abnormal glycan degradation, both of which align with the characteristic biochemical features of V-ATPase-related dysfunction. In addition, they are comparable to those seen in ATP6AP2-CDG patients reported previously by Rujano et al., and indicate a type II CDG pattern [7].

ApoC-III IEF (P1 and P2) and 2-DE (P3 and P4) revealed clear apoC-III $_1$ profiles (Figure 4B and Table 3), consistent with altered protein mucin-type O-glycosylation related to a Golgi V-ATPase defect. 2-DE of serum haptoglobin in P3 and P4 also revealed a pattern compatible with type II CDG, with an additional spot of cathodal migration for both patients, evocative of sialic acid loss (Figure 4C).

Additionally, serum N-glycome following PNGase treatment was performed in P3 and P4. These were also consistent with a type II CDG. Methods and results are briefly presented in Figure S5.

4 | Discussion

4.1 | Expanding the Spectrum of ATP6AP2-Related Neurological Disease, Including the First Affected Female

Herein, we report four individuals with ATP6AP2 splicing variants and severe neurological and developmental symptoms. These affected individuals are clinically unlike previously reported ATP6AP2-CDG patients (Table 1); however, the presence of N- and O-glycosylation defects allowed us to classify these individuals as affected with CDG (Figure 4). In all individuals, decreased wild-type, full-length ATP6AP2 protein level was observed in fibroblasts (Figures 1-3). Residual full-length ATP6AP2 mRNA levels, taken as a ratio of full-length to exon-skipped reads on RNA-Seq analysis, were comparable in P1 and P2 to a previously reported MRXSH patient with a similar clinical presentation [36]. Remarkably, P4, the first female described with ATP6AP2related inherited disease, was affected, with a milder phenotype compared to her severely affected brother. Importantly, besides this ATP6AP2-CDG affected female, heterozygotes of X-linked ATP6AP1-CDG can also present with an attenuated phenotype

TABLE 2 | Overview of detailed mass spectrometry-detected glycoforms of intact transferrin for all patients.

Mass intact transferrin (amu)	Tentative schematic visualization	Patient 1 (%)	Patient 2 (%)	Patient 3 (%)	Patient 4 (%)	Control (%)
78357		0.5	ND	ND	ND	0
78 648		1.5	ND	ND	ND	0
78811		3.6	1.2	ND	0.5	0
78 974		5.8	4.6	1.2	1.6	0
79 103		5.3	2.2	1.5	ND	0
79 264		29.6	34.9	8.8	14.1	<8%

Note: The schematic visualization represents tentative compositions for the detected masses. Percentages are normalized to the tetrasialylated intact transferrin. All glycoforms, except for the mass at 79 264 Da, are absent in control samples. For the 79 264 Da mass, the percentage in controls is below 8%. Abbreviations: Amu, atomic mass unit; ND, not detected.

consisting of mild proteinuria [37]. To our knowledge, pathogenic *ATP6AP2* variants leading to skipping of exon 5 (as in P1) or introduction of a pseudoexon between exons 6 and 7 (as in P3 and P4) have not previously been reported. Our study therefore also expands the genetic spectrum of ATP6AP2-related disease.

4.2 | The Unique Gene Dosage Sensitivity of *ATP6AP2*

Strikingly, in GnomAD, as well as in affected ATP6AP2-CDG patients, there are no nonsense, frameshift, canonical splice variants or large deletions that could be expected to significantly affect protein function of ATP6AP2. Severe X-linked syndromes are typically described with loss-of-function variants restricted to females or mosaic males (e.g., CASK, MECP2, NEMO, PORCN, DDX3X) [38]. This could suggest that ATP6AP2 loss-of-function variants are prenatally lethal even in heterozygous females. To our knowledge, this is a unique situation in X-linked disease and an indication of the importance of tightly controlled ATP6AP2 levels to the assembly and function of the V-ATPase complex, as well as the importance of the V-ATPase complex itself to human development and health. Notably, P4, a female, had skewed but incomplete (82%-18%) X-inactivation in PBMC. We propose that the isolated neurological phenotype in patients with ATP6AP2 splice variants, as opposed to the liver phenotype in patients with missense variants, is likely due to an extreme gene dosage sensitivity of ATP6AP2 particularly within neurodevelopment.

This is supported by data from Hirose *et al.*, and has also been suggested by Edelman *et al.* in their report of a patient carrying the c.168+6T>A leading to increased skipping of exon 2 [39, 40]. Our findings support the major conclusion of Edelman *et al.*: reduced gene dosage is the main mechanism of disease in ATP6AP2-related disease caused by splicing variants.

4.3 | What Mechanisms Could Explain the Variety of Phenotypes Between ATP6AP2-Related Diseases?

Rujano *et al.* hypothesized that residual levels of wild-type, full-length ATP6AP2 protein was the major determinant of clinical severity, with splicing variants resulting in milder phenotypes due to lower penetrance [7]. However, reported ATP6AP2-CDG patients with missense variants have only mild (or even absent) neurological/developmental symptoms, as opposed to affected individuals with splicing variants, in whom very severe neurological/developmental symptoms are described in the (quasi-)absence of other symptoms [36].

The effect of each variant on protein structure/function explains this heterogeneity of phenotypes, likely derived from residual levels of both protein and transcript. Rujano *et al.* showed that the Arg71His and Leu98Ser missense variants (both in exon 3) lead to reduced interaction of ATP6AP2 with its binding partner, ATP6AP1, unlike the exon 4-skipping variant reported by Korvatska *et al.* [7]. Furthermore, Hirose *et al.* demonstrated that exon 4 inclusion was

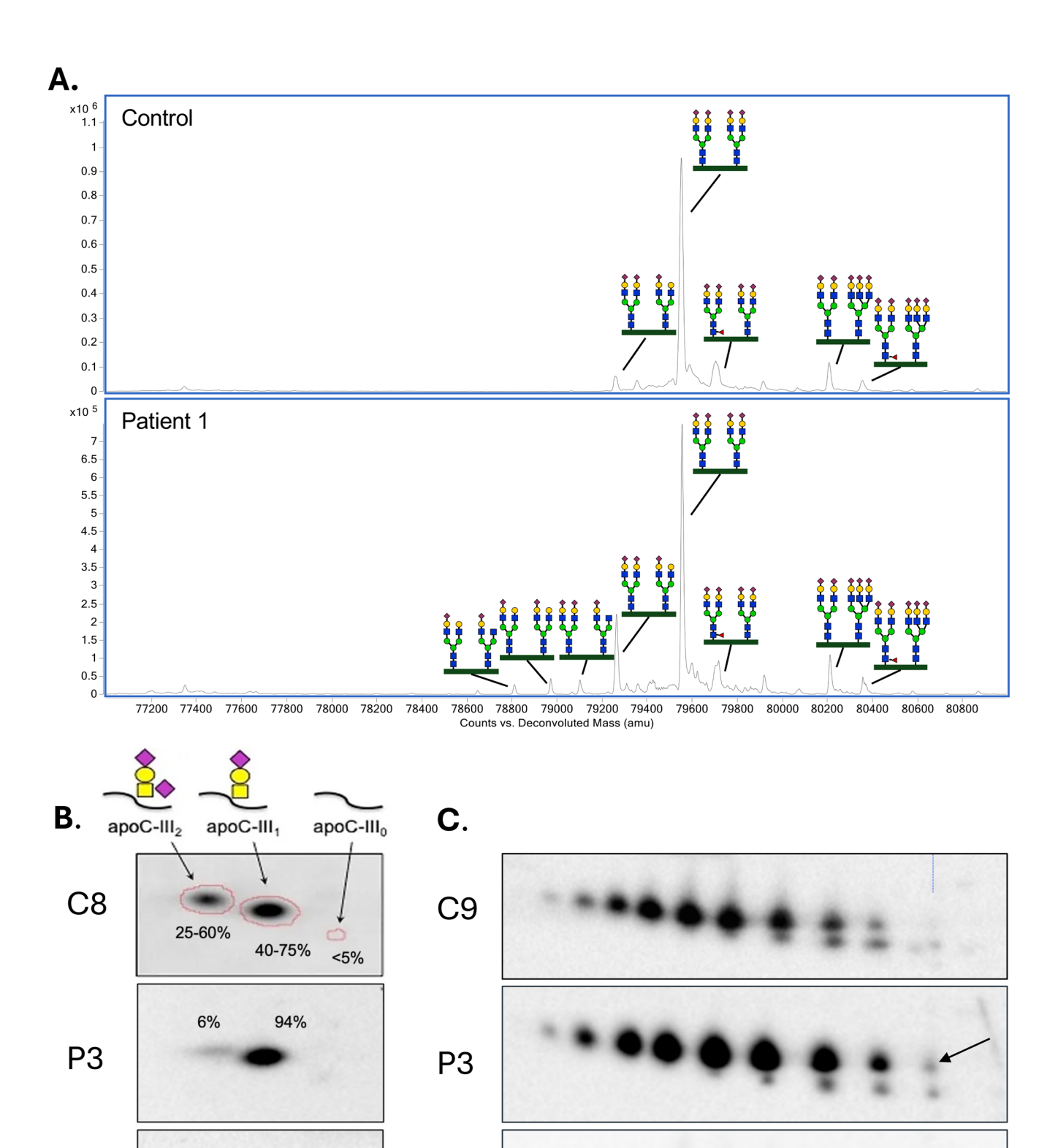


FIGURE 4 | Legend on next page.

P4

MW

10%

90%

P4

MW

charge

FIGURE 4 | Glycosylation studies in the affected individuals reveal abnormal N- and O-glycosylation. (A) Intact transferrin profiles derived from plasma from P1 revealed a profile associated with defects in the V-ATPase with losses of sialic acid and galactose (amu = atomic mass unit). (B) Serum apoC-III two-dimensional electrophoresis performed in P3 and P4 reveal typical apoC-III, profiles, with an increased monosialylated apoC-III glycoform, and a decreased disialylated apoC-III glycoform. These profiles were consistent with abnormal protein mucin-type O-glycosylation related to Golgi V-ATPase dysfunction. A control serum is also presented (C7). (C) Two-dimensional electrophoresis of serum haptoglobin in a control and P3 and P4. The arrows point to additional spots of cathodal migration, evoking loss of sialic acid(s).

critical for survival of iPSC-derived neurons [36]. It appears that point mutations (largely missense) in genes encoding ATP6AP2 and other V-ATPase subunits tend to lead to only mild neurological symptoms and the effect on protein levels are variable [5, 41, 42]. The clinical picture in ATP6AP2-related disease caused by altered splicing seems instead to be limited to neurological tissues. This suggests that transcript/protein level depletion is the major factor underlying the pathology in these patients, and may also explain the variability in affected organs. Korvatska et al. hypothesized that cis-acting splicing regulators could affect the penetrance of splicing variants differently among tissues and stages of development, explaining the phenotypic differences between XPDS and MRXSH affected individuals [4]. Additionally, Ondrusokva et al. reported, in 2020, a case of ATP6AP1-CDG in whom study of brain, fibroblasts and liver autopsy extracts showed differences in protein level and glycosylation among tissues [43]. There is a remarkable similarity in the phenotypic spectra of ATP6AP2-CDG and ATP6AP1-CDG, with the latter also leading to a disorder ranging from isolated liver disease to severe intellectual disability and variable glycosylation defects [34, 44-47].

We show that, as well as reduced wild-type ATP6AP2 protein, additional bands were present by immunoblotting in P1 and P2, evidence of stable truncated ATP6AP2 protein that has escaped ER-associated degradation (Figure 3B). It is possible that, as well as simply the lack of full-length protein, there is a deleterious effect of these truncated transcripts.

4.4 | Is Disrupted Glycosylation a Consistent Feature of Pathogenic ATP6AP2 Variants?

Apart from individuals affected by ATP6AP2-CDG, a very mild glycosylation defect was observed in a prior XPDS-affected individual with an exon 4 skipping variant [7]. Other XPDS and MRXSH patients, to our knowledge, were not tested for abnormal glycosylation, since before 2017 ATP6AP2 variants had not been linked to a CDG. Importantly, glycosylation defects were observed in all affected individuals described here, including a heterozygous female, with splicing variants affecting three different regions of the ATP6AP2 gene. It is therefore possible that defective glycosylation is part of the pathological mechanism of all ATP6AP2-related diseases, as well as other V-ATPase defects, but unlikely that it is the main driver of the neurological pathology given that the glycosylation defects in patients with severe ID/DD in this study were relatively mild. This is logical, given the importance of the V-ATPase proton pump in various aspects of cell biology (e.g., subcellular transport/trafficking) and the well-known sensitivity of neurodevelopment to V-ATPase dysfunction [13]. Of note, the description of glycosylation defects in the "splicing" forms of ATP6AP2-related diseases suggests they are also metabolic diseases in nature.

TABLE 3 | Results of serum apoC-III isoelectric focusing (IEF) in patients 1 and 2 (P1 and P2).

ApoC-III isoform	Patient 1 (P1) (%)	Patient 2 (P2) (%)	Control (%)
0	5.2	3.5	1.4-9.5
1	79.4	83.6	48.5-75.2
2	15.5	13.0	21.0-45.8

Note: Serum apoC-III IEF in P1 and P2 showed apoC-III $_1$ profiles characterized by an increase in the monosialylated apoC-III glycoform (apoC-III $_1$) and a decrease in the disialylated apoC-III glycoform (apoC-III $_2$), apoC-III: Apolipoprotein C-III.

Together, these observations bring us to suggest a clinical spectrum of ATP6AP2-related disease in Figure 5, (i) the amount of residual protein, (ii) specific molecular and/or tissue-specific effects of variants. We are, however, still unable to reconcile differences between the predominant parkinsonism of XPDS, and ID/DD in MRXSH.

4.5 | Usefulness of RNA-Seq Data in the Interpretation of Potential Splicing Variants Identified via Exome or Genome Sequencing

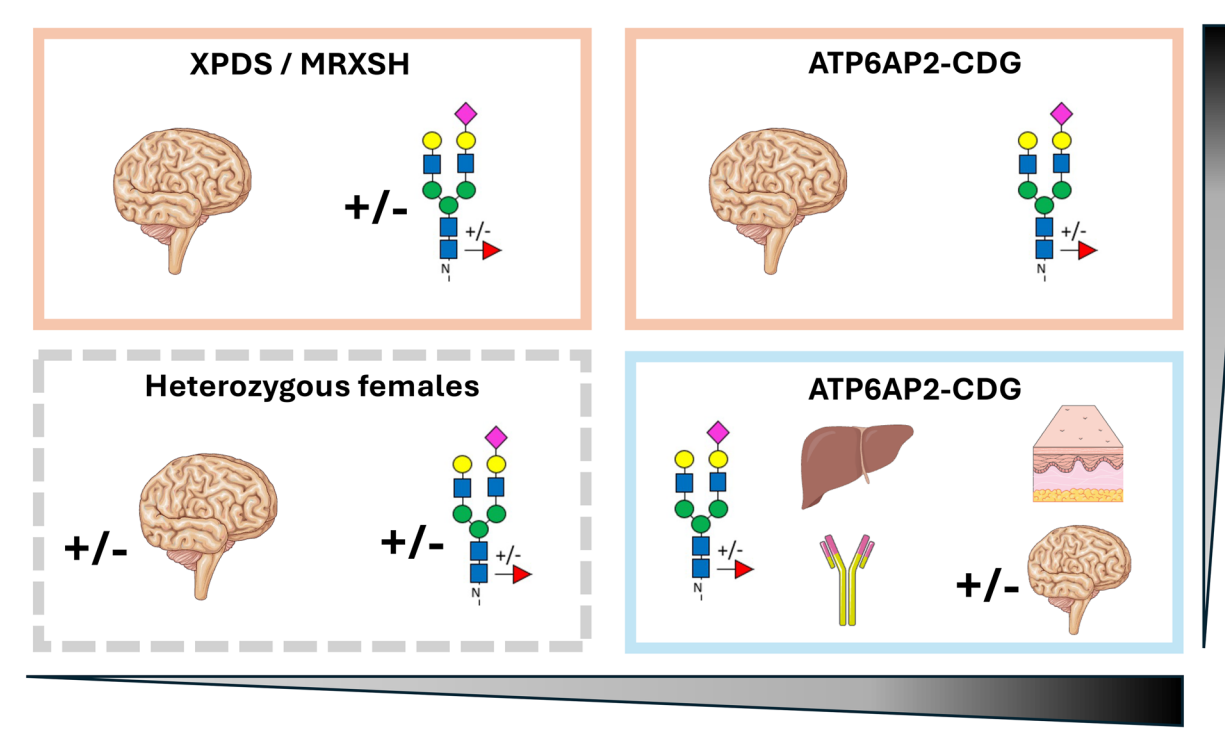
Independently of discussion on ATP6AP2-CDG and related conditions, this work also confirms the usefulness of coupling genomic data with RNA-Seq results for the rapid clinical interpretation of splice variants. In the four individuals we reported, there appears to be a significant correlation between the clinical presentations and the level of abnormal mRNA and protein (e.g., in P1 and P4; Figures 2 and 3; Table 1), contributing to the classification of the different splice variants. This study corroborates once again the potential of coupling genomics and RNA-Seq, previously commented on by other authors [34, 48, 49].

5 | Conclusion

We expand the phenotypic spectrum of the disease, report the first affected female, and conclusively tie together ATP6AP2-related disorders by implicating defective glycosylation as a pathological mechanism in all subtypes. This also points to the metabolic nature of "splicing" forms of ATP6AP2-related diseases. We hypothesize that both variant type and levels of residual fully functional ATP6AP2 proteins may explain the diversity of phenotypes associated with ATP6AP2 pathogenic variants. This is likely linked to the extreme sensitivity of ATP6AP2 to gene dosage effects and loss-of-function variants. Finally, our results corroborate previous observations by other teams that

15732665, 2025, 6, Downloaded from https://onlinelibrary.wiley.com/doi/10.1002/jimd.70109 by Assistance Publique Hopitaux De Paris Ap-Hp, Wiley Online Library on [23/10/2025]. See the Terms

% impaired ATP6AP2/V-ATPase (central nervous system)



% impaired ATP6AP2/V-ATPase (other organs)

Splice variants liver immune system

Missense variants glycosylation CNS skin

FIGURE 5 | Spectrum of ATP6AP2 related conditions. Besides a "dosage effect" (i.e., an association of clinical severity with residual ATP6AP2 protein levels), the various reports of individuals with ATP6AP2-related conditions (XPDS, MRXSH and ATP6AP2-CDG) point to specific molecular effects of the variants. Reported splice variants are associated with mild/severe neurological/developmental phenotypes, while missense variants seem to produce multi-systemic phenotypes, with less severe neurological/developmental symptoms. Abbreviations: CDG: congenital disorder of glycosylation; CNS: central nervous system; MRXSH: syndromic X-linked intellectual disability Hedera type; XPDS: X-linked parkinsonism with spasticity.

the coupling of RNA-Seq to genomics is useful for the interpretation of splice variants in a clinical setting.

Author Contributions

A.R., J.-M.dS.-A., M.B., I.K., G.M., J.J., D.Q., D.J.L., A.B., and M.P.W.: conceptualization. G.M., D.J.L., A.B., and M.P.W.: funding acquisition. A.R., M.A.P., F.K., K.H., A.C., P.B., T.D., E.S., S.C., F.F., E.L., I.C., A.R., E.J., and M.P.W.: investigation/methodology. G.M., A.B.: supervision. A.R., J.-M.dS.-A., M.A.P., M.B., J.J., D.Q., D.J.L., A.B., and M.P.W.: writing – original draft. A.R., J.-M.dS.-A., M.A.P., M.B., I.K., E.S., E.J., K.P., G.M., J.J., D.Q., D.J.L., A.B., and M.P.W.: writing – review and editing.

Acknowledgments

We would like to thank Wim Huybrechts and Liesbeth Keldermans of UZ Leuven, Belgium, for their technical assistance.

Ethics Statement

Research on human material was approved by the ethical committee of the University Hospital Leuven (Study numbers S58358 or S68743). The institutional ethical review committee CMO Radboudumc, Nijmegen, the Netherlands has given approval to conduct studies with leftover diagnostic patient material (CMO Radboudumc dossier number: 2019-5591 and 2020-6588).

Consent

Written informed consent was obtained from the individuals involved in this study or their guardians.

Conflicts of Interest

The authors declare no conflicts of interest.

Data Availability Statement

The data that supports the findings of this study is available in the Supporting Information of this article.

References

1. R. Francisco, S. Brasil, J. Poejo, et al., "Congenital Disorders of Glycosylation (CDG): State of the Art in 2022," *Orphanet Journal of Rare Diseases* 18 (2023): 329.

2. A. F. Eaton, M. Merkulova, and D. Brown, "The H+-ATPase (V-ATPase): From Proton Pump to Signaling Complex in Health and

of use; OA articles are governed by the applicable Creative Commons

- Disease," American Journal of Physiology. Cell Physiology 320 (2021): C392-C414.
- 3. E. J. R. Jansen, S. Timal, M. Ryan, et al., "ATP6AP1 Deficiency Causes an Immunodeficiency With Hepatopathy, Cognitive Impairment and Abnormal Protein Glycosylation," *Nature Communications* 7 (2016): 11600.
- 4. O. Korvatska, N. S. Strand, J. D. Berndt, et al., "Altered Splicing of ATP6AP2 Causes X-Linked Parkinsonism With Spasticity (XPDS)," *Human Molecular Genetics* 22 (2013): 3259–3268.
- 5. U. Kornak, E. Reynders, A. Dimopoulou, et al., "Impaired Glycosylation and Cutis Laxa Caused by Mutations in the Vesicular H+-ATPase Subunit ATP6V0A2," *Nature Genetics* 40 (2008): 32–34.
- 6. T. Van Damme, T. Gardeitchik, M. Mohamed, et al., "Mutations in ATP6V1E1 or ATP6V1A Cause Autosomal-Recessive Cutis Laxa," *American Journal of Human Genetics* 100 (2017): 216–227.
- 7. M. A. Rujano, M. Cannata Serio, G. Panasyuk, et al., "Mutations in the X-Linked ATP6AP2 Cause a Glycosylation Disorder With Autophagic Defects," *Journal of Experimental Medicine* 214 (2017): 3707–3729.
- 8. P. Hedera, D. Alvarado, A. Beydoun, and J. K. Fink, "Novel Mental Retardation-Epilepsy Syndrome Linked to Xp21.1–p11.4," *Annals of Neurology* 51 (2002): 45–50.
- 9. L. C. Bott, M. Forouhan, M. Lieto, et al., "Variants in ATP6V0A1 Cause Progressive Myoclonus Epilepsy and Developmental and Epileptic Encephalopathy," *Brain Communication* 3 (2021): fcab245.
- 10. M. Girard, A. Poujois, M. Fabre, et al., "CCDC115-CDG: A New Rare and Misleading Inherited Cause of Liver Disease," *Molecular Genetics and Metabolism* 124 (2018): 228–235.
- 11. J. C. Jansen, S. Timal, M. van Scherpenzeel, et al., "TMEM199 Deficiency Is a Disorder of Golgi Homeostasis Characterized by Elevated Aminotransferases, Alkaline Phosphatase, and Cholesterol and Abnormal Glycosylation," *American Journal of Human Genetics* 98 (2016): 322–330.
- 12. Y. Fang, Y.-Z. Wang, L. Chen, and X.-B. Xie, "Expanding the Phenotype and Metabolic Basis of ATP6AP2-Congenital Disorder of Glycosylation in a Chinese Patient With a Novel Variant c.185G>A (p.Gly62Glu)," *Frontiers in Genetics* 14 (2023): 1264237.
- 13. A. Falace, G. Volpedo, M. Scala, F. Zara, P. Striano, and A. Fassio, "V-ATPase Dysfunction in the Brain: Genetic Insights and Therapeutic Opportunities," *Cells* 13 (2024): 1441.
- 14. M. Simons, M. Bader, and D. N. Müller, "The (Pro)renin Receptor: What's in a Name?," *Nature Reviews. Nephrology* 16 (2020): 304.
- 15. M. C. Guida, T. Hermle, L. A. Graham, et al., "ATP6AP2 Functions as a V-ATPase Assembly Factor in the Endoplasmic Reticulum," *Molecular Biology of the Cell* 29 (2018): 2156–2164.
- 16. L. Wang, D. Wu, C. V. Robinson, H. Wu, and T.-M. Fu, "Structures of a Complete Human V-ATPase Reveal Mechanisms of Its Assembly," *Molecular Cell* 80 (2020): 501.e3–511.e3.
- 17. M. P. Wilson, D. Quelhas, E. Leão-Teles, et al., "SLC37A4-CDG: Second Patient," *JIMD Report* 58 (2021): 122–128.
- 18. A. Dobin, C. A. Davis, F. Schlesinger, et al., "STAR: Ultrafast Universal RNA-Seq Aligner," *Bioinformatics* 29 (2013): 15–21.
- 19. V. A. Yépez, C. Mertes, M. F. Müller, et al., "Detection of Aberrant Gene Expression Events in RNA Sequencing Data," *Nature Protocols* 16 (2021): 1276–1296.
- 20. H. Thorvaldsdóttir, J. T. Robinson, and J. P. Mesirov, "Integrative Genomics Viewer (IGV): High-Performance Genomics Data Visualization and Exploration," *Briefings in Bioinformatics* 14 (2013): 178–192.
- 21. C. Mertes, I. F. Scheller, V. A. Yépez, et al., "Detection of Aberrant Splicing Events in RNA-Seq Data Using FRASER," *Nature Communications* 12 (2021): 529.

- 22. M. P. Wilson, Z. Durin, Ö. Unal, et al., "CAMLG-CDG: A Novel Congenital Disorder of Glycosylation Linked to Defective Membrane Trafficking," *Human Molecular Genetics* 31 (2022): 2571–2581.
- 23. M. P. Wilson, A. Garanto, F. Pinto e Vairo, et al., "Active Site Variants in STT3A Cause a Dominant Type I Congenital Disorder of Glycosylation With Neuromusculoskeletal Findings," *American Journal of Human Genetics* 108 (2021): 2130–2144.
- 24. M. van Scherpenzeel, G. Steenbergen, E. Morava, R. A. Wevers, and D. J. Lefeber, "High-Resolution Mass Spectrometry Glycoprofiling of Intact Transferrin for Diagnosis and Subtype Identification in the Congenital Disorders of Glycosylation," *Journal of Laboratory and Clinical Medicine* 166 (2015): 639–649.
- 25. A. Bruneel, F. Habarou, T. Stojkovic, et al., "Two-Dimensional Electrophoresis Highlights Haptoglobin Beta Chain as an Additional Biomarker of Congenital Disorders of Glycosylation," *Clinica Chimica Acta* 470 (2017): 70–74.
- 26. P. T. A. Linders, E. C. F. Gerretsen, A. Ashikov, et al., "Congenital Disorder of Glycosylation Caused by Starting Site-Specific Variant in Syntaxin-5," *Nature Communications* 12 (2021): 6227.
- 27. A. Bruneel, T. Robert, D. J. Lefeber, et al., "Two-Dimensional Gel Electrophoresis of Apolipoprotein C-III and Other Serum Glycoproteins for the Combined Screening of Human Congenital Disorders of O- and N-Glycosylation," *PROTEOMICS Clinical Applications* 1 (2007): 321–324.
- 28. S. Wopereis, D. J. Lefeber, E. Morava, and R. A. Wevers, "Mechanisms in Protein O-Glycan Biosynthesis and Clinical and Molecular Aspects of Protein O-Glycan Biosynthesis Defects: A Review," *Clinical Chemistry* 52 (2006): 574–600.
- 29. S. Yen-Nicolaÿ, C. Boursier, M. Rio, et al., "MALDI-TOF MS Applied to apoC-III Glycoforms of Patients With Congenital Disorders Affecting O-Glycosylation. Comparison With Two-Dimensional Electrophoresis," *Proteomics. Clinical Applications* 9 (2015): 787–793.
- 30. Y. Liang, L. Wan, H. Yan, et al., "Synonymous Variants in the AT-P6AP2 Gene May Lead to Developmental and Epileptic Encephalopathy," *Frontiers in Neurology* 14 (2023): 1320514.
- 31. C. Cousin, D. Bracquart, A. Contrepas, P. Corvol, L. Muller, and G. Nguyen, "Soluble Form of the (Pro)renin Receptor Generated by Intracellular Cleavage by Furin Is Secreted in Plasma," *Hypertension* 53 (2009): 1077–1082.
- 32. K. Ohba, M. Endo, S. Sato, Y. Kashio-Yokota, T. Hirose, and K. Takahashi, "(Pro)renin Receptor/ATP6AP2 Is Required for Autophagy and Regulates Proliferation in Lung Adenocarcinoma Cells," *Genes to Cells* 25 (2020): 782–795.
- 33. S. Kissing, S. Rudnik, M. Damme, et al., "Disruption of the Vacuolar-Type H+-ATPase Complex in Liver Causes MTORC1-Independent Accumulation of Autophagic Vacuoles and Lysosomes," *Autophagy* 13 (2017): 670–685.
- 34. B. Morales-Romero, G. Muñoz-Pujol, R. Artuch, et al., "Genome and RNA Sequencing Were Essential to Reveal Cryptic Intronic Variants Associated to Defective ATP6AP1 mRNA Processing," *Molecular Genetics and Metabolism* 142 (2024): 108511.
- 35. N. Abu Bakar, D. J. Lefeber, and M. van Scherpenzeel, "Clinical Glycomics for the Diagnosis of Congenital Disorders of Glycosylation," *Journal of Inherited Metabolic Disease* 41 (2018): 499–513.
- 36. T. Hirose, A. Cabrera-Socorro, D. Chitayat, et al., "ATP6AP2 Variant Impairs CNS Development and Neuronal Survival to Cause Fulminant Neurodegeneration," *Journal of Clinical Investigation* 129 (2019): 2145–2162.
- 37. P. Lipiński, D. Rokicki, A. Bogdańska, J. Lesiak, D. J. Lefeber, and A. Tylki-Szymańska, "ATP6AP1-CDG: Follow-Up and Female Phenotype," *JIMD Report* 53 (2020): 80–82.
- 38. B. R. Migeon, "X-Linked Diseases: Susceptible Females," Official Journal of the American College of Medical Genetics 22 (2020): 1156–1174.

- 39. W. C. Edelman, K. Kiianitsa, T. Virmani, et al., "Reduced Gene Dosage Is a Common Mechanism of Neuropathologies Caused by ATP6AP2 Splicing Mutations," *Parkinsonism & Related Disorders* 101 (2022): 31–38.
- 40. H. V. Gupta, J. Vengoechea, K. Sahaya, and T. Virmani, "A Splice Site Mutation in ATP6AP2 Causes X-Linked Intellectual Disability, Epilepsy, and Parkinsonism," *Parkinsonism & Related Disorders* 21 (2015): 1473–1475.
- 41. S. Esmail, N. Kartner, Y. Yao, J. W. Kim, R. A. F. Reithmeier, and M. F. Manolson, "Molecular Mechanisms of Cutis Laxa- and Distal Renal Tubular Acidosis-Causing Mutations in V-ATPase a Subunits, AT-P6V0A2 and ATP6V0A4," *Journal of Biological Chemistry* 293 (2018): 2787–2800.
- 42. E. H. Stover, K. J. Borthwick, C. Bavalia, et al., "Novel ATP6V1B1 and ATP6V0A4 Mutations in Autosomal Recessive Distal Renal Tubular Acidosis With New Evidence for Hearing Loss," *Journal of Medical Genetics* 39 (2002): 796–803.
- 43. N. Ondruskova, T. Honzik, A. Vondrackova, et al., "Severe Phenotype of ATP6AP1-CDG in Two Siblings With a Novel Mutation Leading to a Differential Tissue-Specific ATP6AP1 Protein Pattern, Cellular Oxidative Stress and Hepatic Copper Accumulation," *Journal of Inherited Metabolic Disease* 43 (2020): 694–700.
- 44. N. Semenova, O. Shatokhina, O. Shchagina, et al., "Clinical Presentation of a Patient With a Congenital Disorder of Glycosylation, Type IIs (ATP6AP1), and Liver Transplantation," *International Journal of Molecular Sciences* 24 (2023): 7449.
- 45. H. Alharbi, E. J. P. Daniel, J. Thies, et al., "Fractionated Plasma N-Glycan Profiling of Novel Cohort of ATP6AP1-CDG Subjects Identifies Phenotypic Association," *Journal of Inherited Metabolic Disease* 46 (2023): 300–312.
- 46. S. Barua, S. Berger, E. M. Pereira, and V. Jobanputra, "Expanding the Phenotype of ATP6AP1 Deficiency," *Cold Spring Harbor Molecular Case Studies* 8 (2022): a006195.
- 47. B. Dimitrov, N. Himmelreich, A. L. Hipgrave Ederveen, et al., "Cutis Laxa, Exocrine Pancreatic Insufficiency and Altered Cellular Metabolomics as Additional Symptoms in a New Patient With ATP6AP1-CDG," *Molecular Genetics and Metabolism* 123 (2018): 364–374.
- 48. R. Bronstein, E. E. Capowski, S. Mehrotra, et al., "A Combined RNA-Seq and Whole Genome Sequencing Approach for Identification of Non-Coding Pathogenic Variants in Single Families," *Human Molecular Genetics* 29 (2020): 967–979.
- 49. N. M. Ferraro, B. J. Strober, J. Einson, et al., "Transcriptomic Signatures Across Human Tissues Identify Functional Rare Genetic Variation," *Science* 369 (2020): eaaz5900.

Supporting Information

Additional supporting information can be found online in the Supporting Information section. Figure S1: Images of patients 2 and 4 (P2 and P4). Figure S2: (A) ATP6AP2 MANE transcript NM_003765 with locations of primer sets 1 and 2, used for panels S2A and S2B, respectively. (B) Expression of ATP6AP2 measured using primer set 1, showing a mean expression of 62% compared to the mean of Ctrls 5-7. (C) Expression of ATP6AP2 measured using primer set 2, showing expression of 4% compared to the mean of controls 5-7. All N=3, Statistical testing performed by a one-way ANOVA followed by a Tukey's multiple comparisons test. **** = p < 0.0001. Sequences of primers used can be found in Table S2. Figure S3: Uncropped images of immunoblotting results presented in Figure 3A,B. Figure S4: (A) Western-blot of LC-I and LC-II in cultured fibroblasts from P3 by comparison with two controls; n = 3; Errors bars = SEM. BafA1: V-ATPase inhibitor; PP242: mTor inhibitor. (B) Corresponding statistical analysis of HSC70-normalized LC3-II/ LC3-I ratios in P3 and controls. Figure S5: MALDI-TOF mass spectra of permethylated PNGase F-released N-glycans from a healthy subject and P3 and P4. Measurements were performed in the positive-ion mode and all ions are present in sodiated form [M+Na]⁺. Green circles, mannose; yellow circles, galactose; blue squares, *N*-acetyl-glucosamine; red triangles, fucose; purple diamonds, sialic acid. **Table S1:** Antibodies used for immunoblotting. **Table S2:** List of primers used for RT-qPCR.